Raman scattering and far-infrared studies of the vanadium dihalides with layered structure

W. Bauhofer, G. Güntherodt,* E. Anastassakis,† A. Frey, and G. Benedek ‡
Max-Planck-Institut für Festkörperforschung, Heisenbergstasse 1, 7000 Stuttgart 80, Federal Republic of Germany
(Received 16 June 1980)

The vanadium dihalides with layered structure, VCl_2, VBr_2, and VI_2, have been investigated by Raman and infrared spectroscopy. A compilation of the measured optical frequencies is given. The new lines appearing in the Raman spectrum of VI_2 below its Néel temperature T_N are attributed to zone-boundary-phonon Raman scattering induced by Bragg scattering from the spin superstructure. We discuss the symmetry properties and selection rules for the proposed spin-dependent electron-phonon coupling mechanism due to a phonon modulation of the exchange interaction. The measured two-phonon absorption spectra of the three materials show a shift to lower frequencies with respect to the calculated two-phonon density of states. Some possible reasons for this unusually large shift are discussed. The Raman spectra of VCl_2 and VBr_2 show additional features at low temperature, different from the sharp lines observed in VI_2 below T_N. This additional scattering is also shifted to lower frequencies compared to the calculated one-phonon density of states. We explain the appearance of the additional Raman scattering by a spin-phonon coupling via the exchange modulation mechanism, whereas the shift in the Raman spectra should be due to a self-energy renormalization by the coupling mechanism.

I. INTRODUCTION

In recent years, several $3d$-metal dihalides with layered structure have been investigated by Raman spectroscopy.[1–7] Besides a determination of the frequencies of the Raman-active phonons, these studies were aimed at exploring the ground state of the metal ion by electronic Raman scattering[2–4] or at detecting magnons.[5–7] In this work on the vanadium dihalides with layered structure VX_2 (X = Cl, Br, I) we have focused our attention on the influence of magnetic order on the phonon Raman scattering. Such a spin-dependent phonon Raman scattering is known to occur in certain rare-earth compounds due to the spin-orbit coupling in the excited intermediate state.[8] However, the spin-orbit coupling constant of $3d$ transition metal ions is smaller than in rare-earth ions by at least one order of magnitude. On the other hand, the larger superexchange in $3d$-metal compounds compared to rare-earth compounds, due to the more extended, partially filled d shells, could provide another mechanism for a spin-phonon coupling through a phonon-modulated exchange interaction. It turns out from symmetry considerations that such coupling can be nonzero only for complex magnetic structures, such as the antiferromagnetic phase of VI_2.[9] In addition, experimental investigations of the vanadium dihalides take advantage of the ($^4A_2$) singlet ground state of the V^{2+} ion which does not cause any interference of electronic and phononic Raman scattering as observed in $FeCl_2$ by Johnstone *et al.*[4] Moreover, the V^{2+} ground state has a quenched orbital angular momentum and we expect no complications due to hybridization at possible crossings of the magnon and phonon dispersion curves, like in $FeCl_2$.[10]

Recent advances in the crystal growth of VX_2 have provided suitable single crystals for infrared and Raman studies. Details of sample preparation and handling as well as a description of the experimental equipment used in our work are given in Sec. II of this paper.

For an analysis of the additional features observed in the low-temperature Raman data a complete knowledge of the vibrational properties of the materials under investigation is necessary. Phonon dispersion curves have been obtained from a lattice-dynamical calculation based on an extended shell model.[11,12] The parameters for the potential used in this model are either taken from the literature or derived from lattice constants and cohesive energies. The three adjustable parameters (net charge, shell charge, and shell-core displacement of the halogen ion) are fitted to five measured optical frequencies. Section III of this paper deals with the determination of the optical frequencies of VX_2 by means of Raman and far-infrared spectroscopy. In general, the best choice of the parameters leads to an agreement better than 3% between experimental and theoretical frequencies. The validity of the lattice-dynamical model is further confirmed by the excellent agreement between the measured two-phonon infrared transmis-

sion spectra and the calculated two-phonon density of states with respect to their bandwidths and shapes. However, the experimental two-phonon spectra are anomalously shifted to lower frequencies with respect to the theoretical combination bands. We discuss this effect by considering the relevant diagrams for the two-phonon infrared absorption.

In Sec. IV A we present the temperature dependence of the VI_2 Raman spectra. We find three new Raman lines below the antiferromagnetic ordering temperature ($T_N = 15$ K) which we have attributed in a previous letter[13] to a modulation of the magnetic exchange interaction by selected phonon modes. Here, we give a comprehensive description of this spin-phonon coupling mechanism by showing the set of polarization vectors at the relevant points of the Brillouin zone. In addition, we report data on the temperature and magnetic field dependence of the magnetic susceptibility of VI_2 which are the basis of the magnetic phase diagram presently assumed.

The Raman spectra of VBr_2 and VCl_2 and their temperature dependence are discussed in Sec. IV B. Both substances show in addition to the Raman-active modes an anomalous scattering with drastic changes as a function of temperature. Since knowledge of the magnetic properties of VBr_2 and VCl_2 is limited, only a tentative explanation of the observed anomalous features is given. The magnetic susceptibilites of VBr_2 and VCl_2 do not indicate any collective magnetic order down to 5 K.[14,15] However, from the appearance of sharp absorption lines in the visible spectra of VCl_2 below 50 K and of VBr_2 below 30 K which are interpreted as magnon-assisted crystal-field transitions, a short-range magnetic order is inferred. With the assumption of a local magnetic order in VCl_2 and VBr_2 at low temperatures, the same mechanism as in VI_2 should cause the additional Raman scattering. The self-energy renormalization of the phonons due to this spin-phonon coupling mechanism then leads to a shift of the observed scattering spectra with respect to the one-phonon density of states.

II. EXPERIMENTAL DETAILS

Single crystals of VX_2 (X = Cl, Br, I) have been grown from the vapor phase, using the pure elements as starting materials, by G. Lamprecht and E. Schönherr at this institute. Details of the method of preparation will be published elsewhere.[16] Usually the crystals grow in the form of large, thin platelets ($10 \times 10 \times 0.1$ mm^3) perpendicular to the c axis, manifesting the layered character of the structure. VI_2 crystals can be obtained with a thickness of up to 2–3 mm, but the order in the c direction between the I-V-I sandwiches is strongly perturbed, as indicated by broad x-ray reflections. All VX_2 samples reveal a sensitivity to air and moisture which strongly increases towards the heavier halogens. We performed all sample manipulations in a dry argon atmosphere. This was particularly important for getting reproducible Raman spectra of VI_2. The reproducibility of the measurements on different sample batches grown under different conditions strongly reduces the possibility of the occurrence of extrinsic features in the spectra.

The far-ir transmission and reflection spectra were obtained with a Polytec FIR-30 Fourier spectrometer. For the spectra in the visible range a Cary 14 was used. For the far-ir transmission measurements the samples were ground in a powder mill in order to average over all the crystallographic directions. Pellets were pressed from a mixture of powdered polyethylene and the ground sample. Raman spectra were recorded with either a Jarrell Ash or a Spex double monochromator, using a photon counting technique. Ar^+ and Kr^+ ion gas lasers have been used as exciting light sources. The magnetic field dependence of the Raman scattering has been measured using a Thor superconducting magnet with a maximum field of 7 T. The high-field measurements were performed at the Hochfeld-Magnetlabor of the Max-Planck-Institut für Festkörperforschung in Grenoble.

III. FIRST- AND SECOND-ORDER PHONON SPECTRA

A. Zone center phonons

The vanadium dihalides VX_2 (X = Cl, Br, I) crystallize in a layered structure of the CdI_2 type belonging to the trigonal space group D_{3d}^3. This structure consists of hexagonal sheets of metal atoms sandwiched between two hexagonal sheets of anions. The nearest neighbors of a metal atom form a slightly distorted octahedron. A factor group analysis yields four optic modes at the Γ point: $A_{1g} + E_g + A_{2u} + E_u$, i.e., two Raman-active (even) modes and two infrared-active (odd) modes. Figure 1 shows the eigenvectors of the Γ-point normal modes. The atoms vibrate within the layers in the E modes and perpendicular to the layers in the A modes.

Figure 2 shows the room-temperature Raman spectra of the investigated crystals. All spectra had to be taken in the back scattering geometry on very thin samples in order to avoid multiple reflections from the different layers. Right-angle scattering on thick samples could not be carried out since the lamellar structure perpendicular to the c axis prevented any optical polishing. Thus, a complete determination of all Raman tensor components was impossible. However, we can distinguish between parallel and crossed polarizations of the electrical field vectors of incident and scattered light, $z(xx)\bar{z}$ and $z(xy)\bar{z}$, respectively,

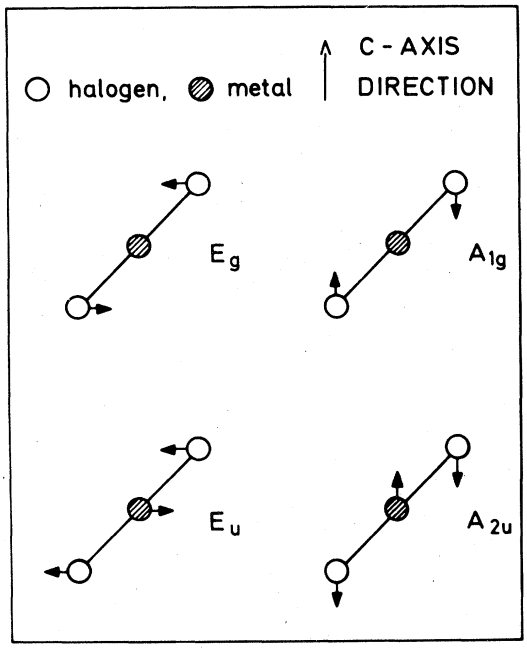

FIG. 1. Eigenvectors of the zone-center optical modes of the CdI_2 structure.

where z refers to the crystallographic c axis. The E_g mode should be unaffected by a change in polarization, whereas the A_{1g} mode should appear only in the parallel scattering configuration. Such a behavior is indeed observed. As in the other $3d$-metal dihalides with layered structure, the A_{1g} mode has the higher frequency compared with the E_g vibration.

For VCl_2 and VI_2 we checked several different exciting laser energies in the range from 2.41 to 2.73 eV in order to optimize the scattering efficiency. After corrections have been made for the instrument function, the ω^4 dependence, and the absorption, the maximum intensity for VCl_2 is obtained at 2.41 eV and for VI_2 at 2.65 eV (at 4 K). Both maxima fall into local minima between two adjacent crystal-field absorption bands.[17] In VCl_2 the intensity variation with incident energy scales inversely with the absorption spectrum. The A_{1g} mode of VI_2, however, exhibits a rather pronounced resonant behavior with a change in scattering intensity, after corrections, by a factor of 15. There is no obvious explanation for this resonancelike behavior, since it occurs in a region of weak $3d$ crystal-field transitions far below the electronic band gap.[17] However, this resonance behavior had only an influence on the scattering intensity, but not on the Raman selection rules.

The two-dimensional character of VX_2 causes some difficulties in determining the infrared-active modes. Because of the above-mentioned difficulties in

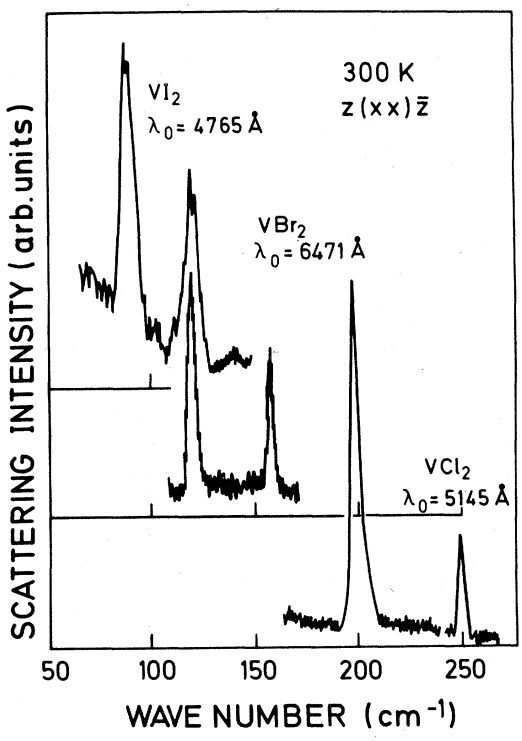

FIG. 2. Room-temperature Raman spectra of the vanadium dihalides.

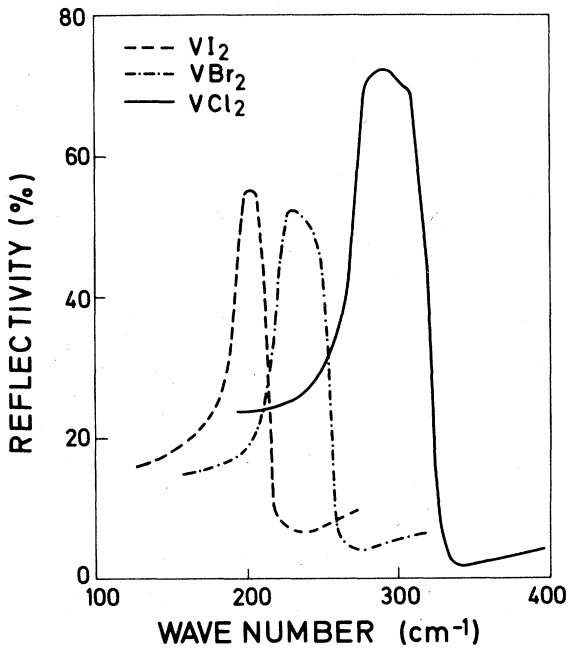

FIG. 3. Infrared reflectivity spectra of the vanadium dihalides at 300 K.

TABLE I. Experimental and theoretical infrared and Raman frequencies (cm^{-1}) at 300 K and calculated ionicities.

	VCl_2		VBr_2		VI_2	
	Expt.	Theor. (Ref. 12)	Expt.	Theor. (Ref. 12)	Expt.	Theor. (Ref. 12)
E_g	198	198	120	122	90	90
A_{1g}	247	242	158	150	115	115
E_u						
TO transm.	275	287	225	232	200	200
KK	286		231		200	
LO KK	325	321	258	250	218	208
A_{2u} (TO) transm.	320	315	261	254	220	220
Net charge (Ref. 12)		0.79		0.79		0.75

preparing samples with a sufficiently large surface parallel to the c axis, only the E_u reststrahlenband is seen in reflectivity measurements as shown in Fig. 3. Via a Kramers-Kronig (KK) analysis we obtained the real (ϵ_1) and the imaginary (ϵ_2) part of the complex dielectric function $\epsilon(\omega)$ and the frequencies of the transverse and longitudinal E_u vibrations using the relations

$$\omega_{TO} = \max(\omega\epsilon_2)$$

and

$$\omega_{LO} = \max\left(\frac{1}{\omega}\mathrm{Im}\epsilon^{-1}\right) .$$

For the determination of the A_{2u} oscillator we performed ir transmission measurements of powdered samples diluted with powdered polyethylene. The grinding procedure is again rendered more difficult because of the layered structure of the samples. Best results were obtained using a powder mill. Figure 4 shows the transmission spectra in the appropriate energy range, clearly revealing the absorption due to the A_{2u}(TO) mode. However, we found no way for an experimental determination of the A_{2u}(LO) frequency.

Table I gives a compilation of the measured frequencies of VX_2 together with the values obtained from the model calculation. The sets of parameters used in the calculation are reported in Ref. 12. Since the model has been especially developed to give reliable values for the net charge, we have included the corresponding numbers for VX_2 in Table I.

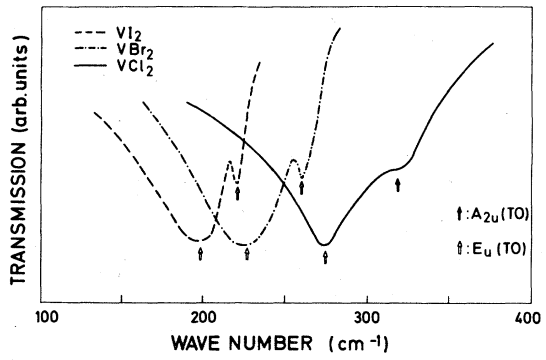

FIG. 4. Infrared transmission spectra of powdered samples of the vanadium dihalides at 300 K.

B. Two-phonon infrared absorption

Figure 5 shows some single crystal far-infrared transmission spectra. Absorption peaks due to two-phonon processes can be observed at the high-frequency side of the main E_u oscillator. These structures have a marked similarity for all three compounds. The appearance of rather sharp two-phonon absorption peaks is a consequence of the small dispersion of the optical branches.

The ($q = 0$) combinations of the calculated branches originating from E_u at Γ with those originating from E_g and A_{1g} at Γ which transform like E_u or A_{2u} irreducible representations yield two-phonon densities ($\rho_{u\times g}$) in good agreement with the observed 5-K spectra (Fig. 6), particularly in what concerns bandwidths and shapes. However, in all three compounds the experimental spectra appear to be shifted to lower frequencies with respect to the region (hatched area) delimited by the lowest, $\omega(E_u, \mathrm{TO}) + \omega(E_g)$, and highest, $\omega(E_u, \mathrm{TO}) + \omega(A_{1g})$, combi-

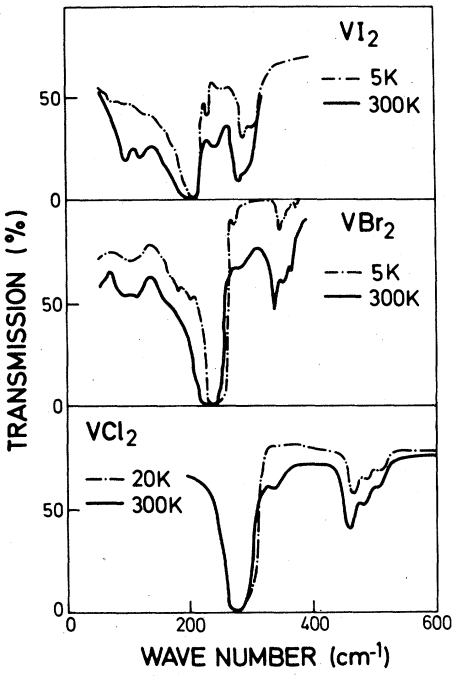

FIG. 5. Single-crystal infrared transmission spectra of the vanadium dihalides as a function of temperature.

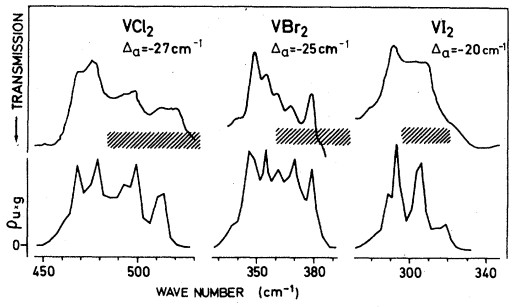

FIG. 6. Comparison of the measured two-phonon absorption spectra of the vanadium dihalides (upper part) with the shifted calculated combinations of even (g) and odd (u) modes. The shift of the calculated two phonon bands to lower frequencies is denoted by Δ_a. The shaded area indicates the interval between the lowest, $E_u + E_g$, and the highest, $E_u + A_{1g}$, combination of measured frequencies.

nation of the experimentally available low-temperature frequencies. The same refers to the calculated densities, which have been shifted in Fig. 6 by $\Delta_a = -20$ cm^{-1} for VI_2 to $\Delta_a = -27$ cm^{-1} for VCl_2. $\rho_{u\times g}$ has been computed using room-temperature frequencies since no 5-K data were available. A calculation for low temperatures would make this shift even larger, but the difference would be within the accuracy of the theory. On the other hand, we want to point out that the hatched areas in Fig. 6 determined from experimental frequencies represent the low-frequency limit of the two-phonon bands since the phonon branches originating from E_u have their minimum frequency at Γ, as can be seen from the calculated dispersion curves in Figs. 7(a), 7(b), and 7(c). The lattice-dynamical model of Ref. 12 has been applied to a number of transition-metal dihalides and the calculated phonon dispersion curves are in good agreement with existing neutron data. Although we cannot rule out completely the possibility of some peculiar effects specific to the vanadium dihalides, we strongly believe in the applicability of the model to these compounds.

Two mechanisms are responsible for the two-phonon infrared absorption in polar crystals.[18] The first is the purely anharmonic mechanism in which the incident photon couples with a TO lattice mode

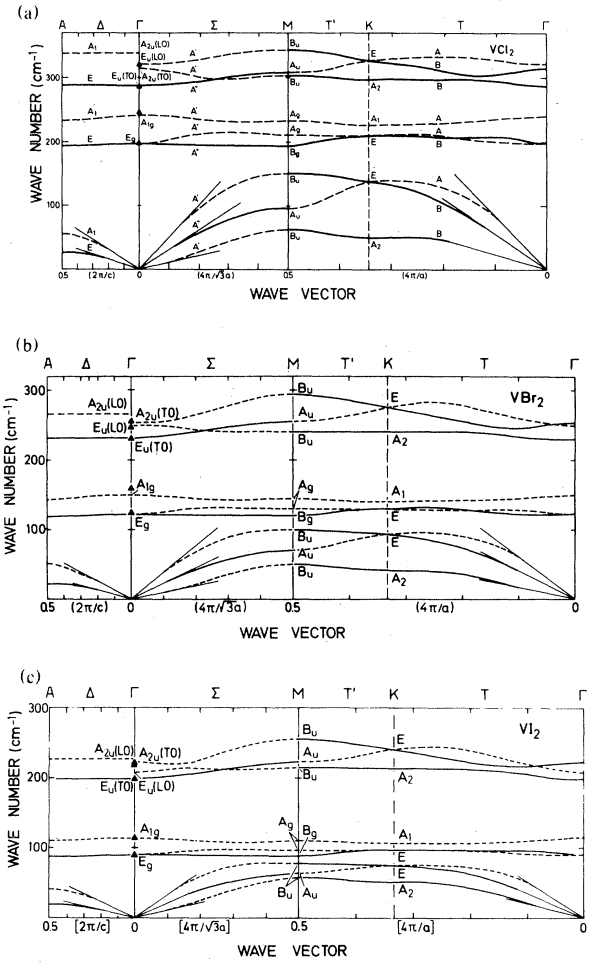

FIG. 7. (a)–(c) Phonon dispersion curves of the vanadium dihalides VX_2 (X = Cl, Br, I) along different symmetry directions. Black triangles represent experimental frequencies.

and phonon sidebands are generated due to cubic anharmonicity. The second mechanism consists of the direct coupling of the photon to a two-phonon state via the second-order dipole moment. The latter mechanism is usually negligible in fully ionic crystals such as alkali halides, but it can be important in crystals combining reduced ionicity with a high anion polarizability. An estimate of the ratio of the second-order dipole moment to the corresponding anharmonic coefficient using Borik's approximate equation[19] gives for the vanadium dihalides a value about five times larger than that for alkali halides. Hence the second-order dipole moment mechanism may play an important role in our present case.

In an approximate calculation of the frequency renormalization due to the second-order dipole moment mechanism we have considered the poles of the imaginary part of the (renormalized) two-phonon propagator

$$G^{(2)}_{\lambda\lambda'}(\omega) = \frac{2(\omega_\lambda+\omega_{\lambda'})(1+n_\lambda+n_{\lambda'})}{(\omega_\lambda+\omega_{\lambda'})^2-(\omega+i0^+)^2} + \frac{2(\omega_\lambda-\omega_{\lambda'})(n_\lambda-n_{\lambda'})}{(\omega_\lambda-\omega_{\lambda'})^2-(\omega+i0^+)^2} , \quad (1)$$

where $\omega_{\lambda(\lambda')}$ and $n_{\lambda(\lambda')}$ are the frequencies and occupation numbers of the phonons, respectively.

The connected diagrams for second-order cubic anharmonicity yield a positive [Fig. 8(a)] and a negative [Fig. 8(b)] self-energy renormalization of the two-phonon energy with respect to the sum of the renormalized (experimental) one-phonon energies.

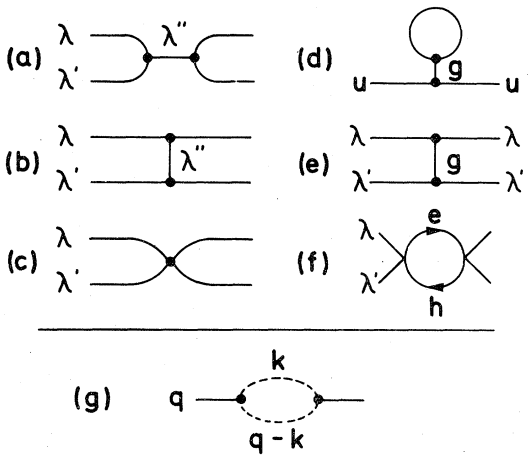

FIG. 8. Diagrams representing two-phonon (a), (b) and one-phonon (c) self-energy contributions due to an anharmonic coupling. The diagrams (d) and (e) could be important in the present case. Diagram (f) shows the two-phonon self-energy contribution arising from the electron two-phonon interaction. Diagram (g) represents the one-phonon self-energy contribution arising from a one-phonon two-magnon process.

The total shift will be negative since there are four diagrams equivalent to Fig. 8(b). Such an effect was already found for resonant modes of strongly anharmonic impurities.[20] When first-order quartic anharmonicity is added [Fig. 8(c)] there is a partial compensation of such a negative shift.

Our calculation shows that the resulting shift is still negative but of the order of a few cm^{-1}. Therefore we do not believe that the considered processes alone can account for the observed effect of more than -20 cm^{-1}. On the other hand, there are some aspects peculiar to layered crystals which could enhance the anharmonic effects. The lack of inversion symmetry at the halogen site yields nonvanishing contributions to the one-phonon and two-phonon self-energy from diagrams (d) and (e) of Fig. 8, where the integral along the intermediate gerade g phonon line is nonvanishing due to the existence of gerade phonons at $q=0$. These contributions could also be important for the anomalously large anharmonic shift observed in the present crystals.

Another possible self-energy correction of the two-phonon energy should not be disregarded, namely, that arising from the second-order electron-phonon interaction. Diagram (f) in Fig. 8 shows an example of this kind of process, which is identical to Borik's[19] second-order dipole moment mechanism.

IV. TEMPERATURE DEPENDENCE OF THE RAMAN SPECTRA

A. VI_2

The temperature dependence of the Raman spectrum of VI_2 in Fig. 9 shows an *abrupt* appearance of three new lines at the frequencies of 66, 195, and 220 cm^{-1} upon cooling below the Néel temperature $T_N = 15$ K. As an example, the temperature dependence of the integrated intensity is shown for the 66-cm^{-1} line in the inset of Fig. 9. The three new lines appear with about the same intensity in the $z(xx)\bar{z}$ and $z(xy)\bar{z}$ scattering configurations. In Ref. 13 we have attributed the three new Raman lines to a folding of the phonon branches according to the magnetic superstructure.[9,21] The microscopic *spin-dependent* electron-phonon interaction has been revealed to be a modulation of the magnetic exchange interaction by selected phonon modes. The interaction Hamiltonian is given by

$$H_{ep} = \frac{1}{2N}\sum_{\vec{q}\lambda} Q_{\vec{q}\lambda}(t)\sum_l e^{i\vec{q}\vec{r}_l} \times \sum_{i\neq j}\left(\sum_\kappa \vec{w}(\kappa|\vec{q}\lambda)\frac{\partial J_{ij}}{\partial \vec{r}_{l\kappa}}\right)\vec{S}_i\vec{S}_j , \quad (2)$$

where $Q_{\vec{q}\lambda}(t)$ and $\vec{w}(\kappa|\vec{q}\lambda)$ are the normal coordi-

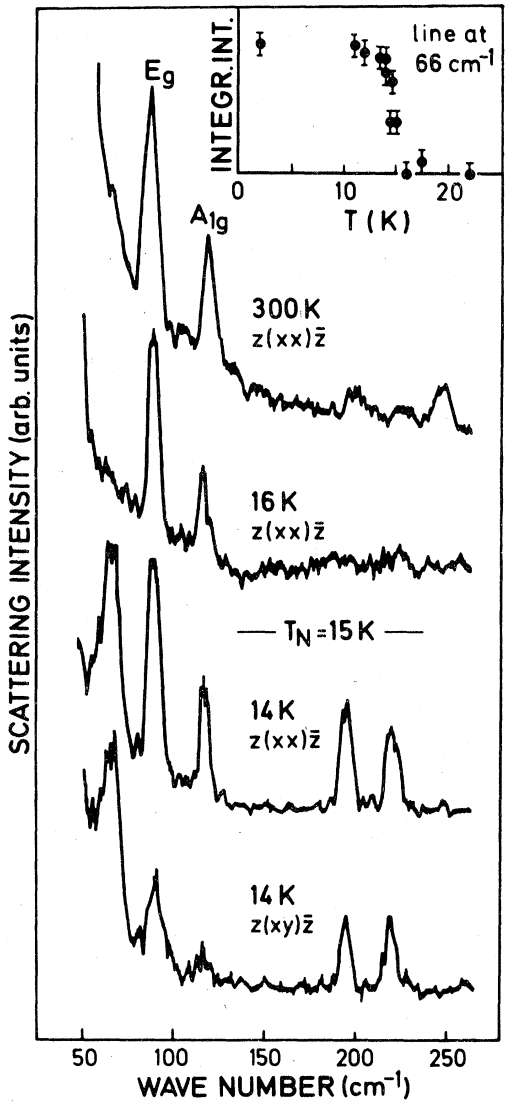

FIG. 9. Raman spectra of VI_2 at different temperatures above and below the Néel temperature. The inset shows the temperature dependence of the integrated intensity of the line at 66 cm^{-1}.

nate operator and the polarization vector, respectively, for wave vector $\vec{q}$ and branch index λ, $\vec{r}_{l\kappa} = \vec{r}_l + \vec{r}_\kappa$ is the position of the κth atom in the lth crystallographic cell ($l = 1, 2, \ldots, N$), and J_{ij} is the exchange constant between spins i and j.

A rough estimate of the coupling strength has shown[13] that the proposed coupling mechanism is of the same order of magnitude as the orbital electron-phonon interaction. In the following we want to outline the inter-relation between the phonon normal coordinates and the spin structure by explicitly summing over the different shells of neighboring spins. For this purpose we assume for the moment that the exchange constant J_{ij} between spins i and j in Eq. (2) depends only on the vanadium-vanadium distance. This assumption does not affect the generality of the symmetry arguments on which our analysis is based. Thus the summation $\sum_{i \neq j}$ in Eq. (2) can be replaced by the following expression

$$\vec{w}(+|\vec{q}\lambda) \sum_n \frac{1}{r_n} \left(\frac{\partial J_n}{\partial r_n} \right) \left[\sum_i^{(n)} \vec{r}_{i,l} \vec{S}_i \vec{S}_l \right] , \tag{3}$$

which has to be summed over all V ions. In Eq. (3) i runs over the nth shell of spins at a distance

$$\vec{r}_n = |\vec{r}_i - \vec{r}_l| = |\vec{r}_{i,l}|$$

around the vanadium site ($\kappa = +$) in cell l. In order to show that a net nonzero phonon modulation of the exchange interaction results, it is sufficient to vary the index l in Eq. (3) over the eight V ions in the magnetic unit cell.

In Fig. 10 we show the projection of the spin superstructure onto the xy plane. The periodicites of the magnetic unit cell are[9,21]: $|\vec{a}_m| = 2|\vec{a}|$, $|\vec{b}_m| = \sqrt{3}|\vec{a}|$. Due to the spin-dependent electron-phonon interaction in the Raman scattering process this magnetic superstructure acts on the phonon system as a folding of phonon branches back into the zone center. The points in the crystallographic Brillouin zone of Fig. 10, subject to the folding, are $\vec{M} = (0, 2\pi/\sqrt{3}a, 0)$, $\vec{K}' = (\pi/a, 0, 0)$ and $\vec{K}''$ (equivalent to $\vec{K}'$). There is an additional periodicity of $2c$ in z direction,[9,21] giving rise to a folding of $\vec{A} = (0, 0, \pi/c)$, $\vec{L}$, $\vec{H}'$, and $\vec{H}''$ (see Fig. 3 of Ref. 13). The sum $\sum_i$ in Eq. (3) has the periodicity of

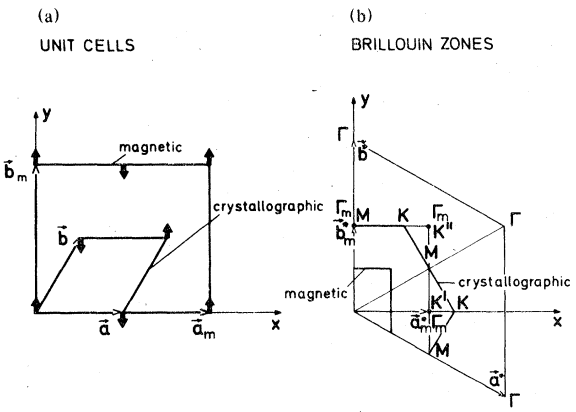

FIG. 10. (a), (b) Projected crystallographic (magnetic) unit cell and Brillouin zone of VI_2 in the paramagnetic (antiferromagnetic) phase. The thick arrows in Fig. 8(a) show the projection of the spin orientation onto the xy plane. The following relations hold: $|\vec{a}_m| = 2a$, $|\vec{b}_m| = \sqrt{3}a$, $|\vec{a}^*| = (4\pi/\sqrt{3}a)$, $|\vec{b}^*| = (4\pi/\sqrt{3}a)$, $|\vec{a}^*_m| = \pi/a$, $|\vec{b}^*_m| = (2\pi/\sqrt{3}a)$, $|\vec{K}'| = |\vec{M}| \cos 30°$, where a is the hexagonal lattice constant.

the magnetic lattice and can be expanded into a finite Fourier series. The latter contains in general $\vec{\Gamma}$ and the above seven reciprocal vectors of the magnetic Brillouin zone. The nonzero Fourier coefficients are found by performing the sum over the actual spin structure. It is sufficient to vary l over the eight spins of the magnetic unit cell and to restrict, for simplicity, the sum over i to the six nearest-neighbor spins.

This has been illustrated in Fig. 11 for two specific spins at positions $l=a$ and $l=c$, where the summations yield

$$\sum_i^{(1)} \vec{\Gamma}_{i,l}\vec{S}_i\vec{S}_l = \begin{cases} 2S^2\vec{\Gamma}_{1,l} = -2S^2(a,0,0), & \text{for } 1=a \text{ or } b \\ -2S^2\vec{\Gamma}_{1,l} = 2S^2(a,0,0), & \text{for } 1=c \text{ or } d \end{cases} . \tag{4}$$

We see that the above vector has only a nonvanishing component along x, which transforms for l, running over the magnetic cell, like the pattern shown in Fig. 11(c).

By inspection of the eigenvectors we can select those modes out of the nine M-point modes which cause a modulation of the exchange interaction. Since the expression in square brackets of Eq. (3) is directed in x direction, all modes which have no component in x direction can be eliminated. As can be seen from Table II, all A_g and B_u modes are discarded in this way. The displacement patterns of the remaining two A_u modes and of the B_g mode are shown in Fig. 12(a)–12(c). The A_u optic mode is mainly a vibration of the metal atoms. We see that for the half-period displayed in Fig. 12(a) the distances of adjacent atoms with antiparallel (parallel) spins increase (decrease), except for those pairs which are aligned along the x axis. The latter are displaced by the same amount in the same direction and give no contribution to the modulation. In the above half-period the overall antiferromagnetic exchange is decreased while the ferromagnetic exchange is increased compared to the equilibrium position. The effect is reversed in the next half-period of the vibration, leading to a modulation of the exchange interaction with the phonon frequency. Figure 12(b) shows that the motion of the iodine atoms in the A_u acous-

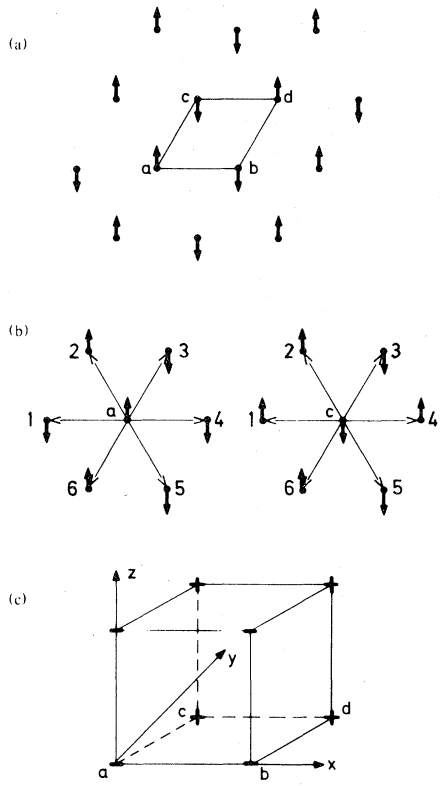

FIG. 11. (a) Spin arrangement of the antiferromagnetic phase of VI_2 projected onto the xy plane; the ions a, b, c, d belong to one unit cell. (b) Nearest neighbors ($n=1$) of spins a and c used for the evaluation of Eq. (3). (c) Sign of the sum in square brackets of Eq. (3) for the eight vanadium sites of the magnetic unit cell.

TABLE II. Eigenvectors of the nine M-point modes within the crystallographic Brillouin zone.

Symmetry	Frequency (cm^{-1})	Iodine (I)			Vanadium (V)			Iodine (I)		
		x	y	z	x	y	z	x	y	z
B_u	255		−0.04	−0.21		0.94	−0.17		−0.04	−0.21
A_u	223	0.25			0.94			0.25		
B_u	215		−0.30	0.04		0.15	0.89		−0.30	0.04
A_g	110		−0.67	0.21					0.67	0.21
A_g	96		−0.21	0.67					0.21	0.67
B_g	88	−0.71						0.71		
B_u	78		0.15	0.66		0.31			0.15	0.66
A_u	63	0.66			−0.35			0.66		
B_u	57		0.62	−0.16		0.06	0.42		0.62	−0.16

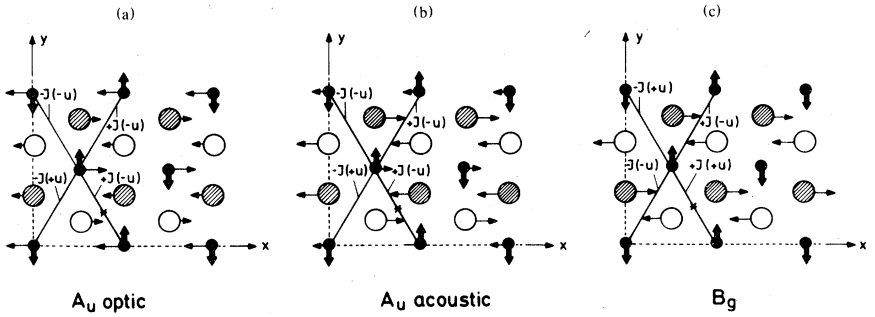

FIG. 12. (a)–(c) Displacement patterns (thin arrows) of the three M-point modes with a nonvanishing x component. Small black circles with thick arrows mark the vanadium ions with their spin direction. The large circles stand for the iodine ions, where the shaded (open) circles are in the plane below (above) the metal sites. The inversion center of the magnetic unit cell is indicated by a star (*).

tic mode enhances the effects produced by the metal ions, since the relative motion of the two iodine atoms responsible for the superexchange between two definite nearest-neighbor spins is in phase with the relative motion of these spins. As concerns the B_g mode [see Fig. 12(c)] no modulation arises either from direct nearest-neighbor exchange, since the metal atoms stay at rest, or from the superexchange via iodine atoms whose contributions cancel each other.

Now we shall discuss the Raman activity and the selection rules for the two A_u modes at M responsible for exchange modulation, as sketched in Ref. 13. The magnetic ordering reduces the original D_{3d} point group symmetry of the crystallographic unit cell to a rhombohedral prism formed by the eight metal sites represented schematically in Fig. 11(c). Disregarding the spin orientations which were only necessary to establish the periodicity of the magnetic unit cell and to determine the phonons active in the exchange modulation mechanism, a c_2 axis along $\langle 1,-3,0\rangle$ and an inversion center at $(\frac{3}{4},\frac{3}{4},\frac{1}{2})$ are retained, forming a C_{2h} subgroup of the original D_{3d} symmetry group. The projection of the inversion center onto the xy plane is indicated by a (*) in Fig. 12. The A_u modes now have even symmetry with respect to this inversion center and are, therefore, Raman active. The even modes A_g and B_g of the C_{2h} point group are polarized along its c_2 axis and perpendicular to it, respectively. Since the polarization of the original A_u modes is along x (the c_2 axis of the C_{2h} group of the M point), forming a 60° angle with the "magnetic" c_2 axis, each A_u mode of the crystallographic unit cell will be transformed into a mixture of A_g and B_g modes of the magnetic unit cell. This fact is reflected by the insensitivity of the observed spectra on the scattering geometry. The calculated frequencies of the two A_u modes at the M point (65 and 223 cm^{-1}) are in very good agreement with the positions of two of the three new Raman lines. The origin of the third line at 195 cm^{-1} is still somewhat puzzling. It could be due to a combination $A_{1g}(\Gamma)+A_u(M)$, which is allowed after the folding of M into Γ. On the other hand, there is still the possibility that, on the basis of the reported periodicities of the magnetic unit cell[9,21] but with slightly different spin orientations, a nonzero modulation is caused by the $E_{u,x}$ mode at the A point, whose frequency (199 cm^{-1}) is very close to the Raman line in question.

We note that the folding of B_g modes of the crystallographic unit cell leads to a combination of infrared-active A_u and B_u modes. However, no additional line is expected in the infrared absorption below T_N, because the B_g mode is unable to modulate the exchange energy [Fig. 12(c)].

The low-temperature Raman spectra of VI_2 (14–2 K) did not show any change in external magnetic fields up to 12 T perpendicular and parallel to the c axis. This is consistent with our investigations of the magnetic phase diagram. The magnetic susceptibility of VI_2 as a function of temperature (at 7 T) is shown in Fig. 13. The Néel temperature of $T_N=15$ K is indicated by the point of inflection on the low-temperature side of the maximum. The transition temperature agrees with that obtained from low-field measurements.[15,22] Only for $T<T_N$, do we observe an anisotropy in the susceptibility for external magnetic fields parallel and perpendicular to the c axis (Fig. 13). This behavior differs from measurements by Kunidersma *et al.*,[9] performed at 0.86 T, showing an increasing anisotropy between $\chi(\|c)$ and $\chi(\perp c)$ for $T<60$ K, with a divergence in $\chi(\|c)$ towards low temperatures. The latter has been attributed to V^{3+} impurities, which seem to be absent in our samples. The much higher magnetic field in our experiments may be the reason for the missing anisotropy for $T>T_N$ (Fig. 13).

The measurements of the magnetization perpendic-

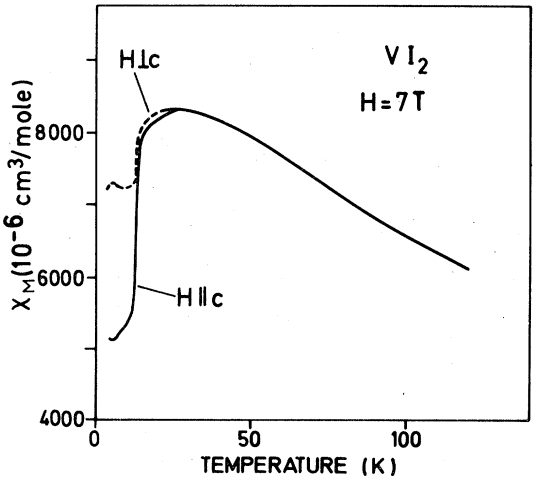

FIG. 13. Magnetic susceptibility at 7 T as a function of the temperature for two different sample orientations.

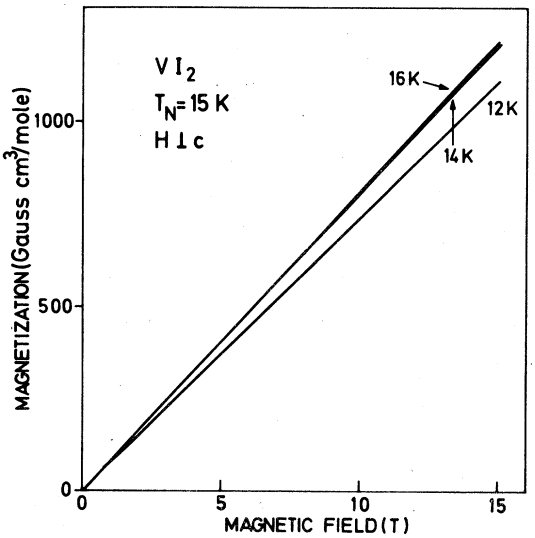

FIG. 14. Magnetization of VI_2 as a function of the applied magnetic field at different temperatures in the vicinity of the Néel temperature $T_N = 15$ K.

ular to c for different temperatures in Fig. 14 show a purely linear dependence on magnetic fields up to 15 T. This behavior clearly indicates the absence of any additional magnetic phase transitions. We conclude that in fields up to 15 T the antiferromagnetic phase is stable and that the spins are not flipped parallel to the external field direction. The decreasing slope of $M(H)$ with decreasing temperature in Fig. 14 is due to the increasing antiferromagnetic ordering, which opposes a canting of the spins towards the external field direction. Within the accuracy of the temperature measurement of ± 1 K the 16- and 14-K data fall into the vicinity of the magnetic phase transition, thus yielding a similar slope. On the other hand, the 12-K data account for the stable antiferromagnetic structure at $T < T_N$.

Kuindersma *et al.*[9] report on an additional magnetic phase at 14.4 K which is regarded as a paramagnetic phase with a high degree of order. The transition from this phase to the antiferromagnetic phase is reported to be about 14 K, which agrees with our value of 15 K within the accuracy of our absolute temperature measurements. In our experiments there is no indication for the occurrence of the intermediate phase. Nevertheless, we have analyzed the 120° spin structure of this phase for the possibility of a phonon modulated exchange interaction.

The 120° structure contains six spins per magnetic cell (three spins in each layer). When the crystallographic Brillouin zone is folded into the magnetic zone, the points A, K, and H are folded into Γ. However, no phonon mode at either the A, K, H, or Γ point yields a nonzero modulation of the exchange interaction. Therefore, no zone-boundary phonon would be activated by the 120° structure. We could only have a weak continuum spectrum induced by the long-range spin disorder. This effect is not detected in VI_2, probably due to the lower signal-to-noise ratio, but seems to be observed in VCl_2 and VBr_2, as discussed in the next section.

B. VBr_2, VCl_2

The prominent features of the room-temperature Raman spectra of VBr_2 and VCl_2 are the two group-theoretically allowed modes (Fig. 2). However, the spectrum of VCl_2 at 300 K in Fig. 15 shows, in addition, a structureless background extending up to about 350 cm^{-1}. This scattering continuum is much larger than the usual background caused by Rayleigh scattering from surface roughness and sample imperfections, but still small compared with the two allowed modes.

The low-temperature Raman spectrum of VBr_2 (see Fig. 16) also shows additional structure whose intensity is comparable to that of the group-theoretically allowed modes, contrary to the case of VCl_2. A similar continuous background scattering as observed at room temperature in VCl_2 is found neither in VBr_2 nor in VI_2. It should be pointed out, however, that the scattering efficiency of VCl_2 is superior to that of VBr_2 and VI_2 for the laser lines used.

The physical nature of the anomalous features in the Raman spectra of VCl_2 and VBr_2 is not yet fully understood. The temperature dependence of the magnetic susceptibility of VCl_2 and VBr_2 shows no clear evidence of a magnetic ordering, but a significant deviation from the linear Curie-Weiss law for temperatures below 100 and 30 K, respectively.[15] In-

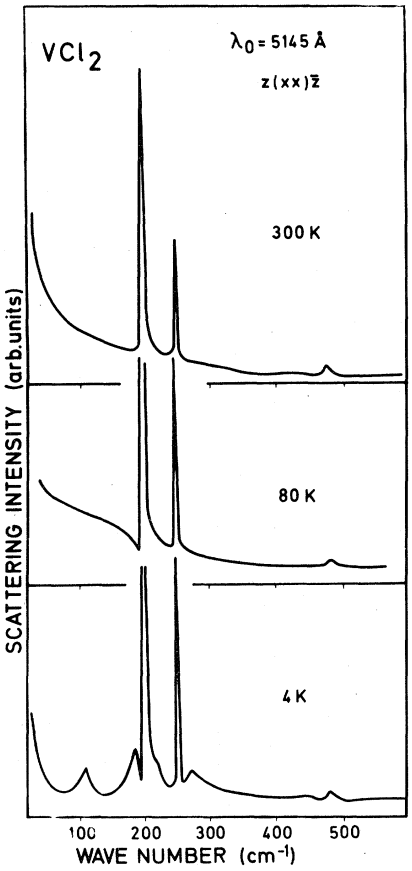

FIG. 15. Raman spectra of VCl_2 at three different temperatures.

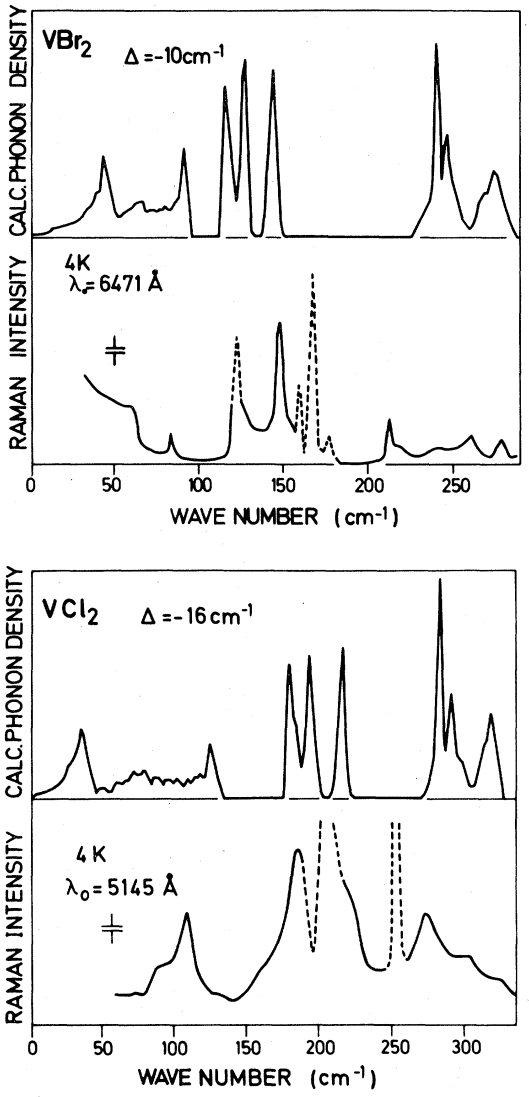

FIG. 16. Comparison of the additional, anomalous low-temperature Raman scattering with a shifted one-phonon density of states for VBr_2 and VCl_2.

terestingly enough, above 50 K in VCl_2 and 30 K in VBr_2 some sharp lines (with a width of a few cm^{-1}) disappear in the visible absorption spectra. Such a behavior is typical for magnon-assisted electric-dipole crystal-field transitions, encountered in many transition-metal compounds in the magnetically orderd phase. As an example for the described behavior, Fig. 17 depicts the temperature dependence of the sharp line at 15 980 cm^{-1} associated with the spin-forbidden $^4A_2 \rightarrow {}^2T_{2g}$ transition of VCl_2.[17,23]

Thus, the susceptibility and the crystal-field-transition data suggest a change in the magnetic properties of VCl_2 and VBr_2 around 50 and 30 K, respectively. Since the anomalous Raman scattering of VCl_2 changes around the same temperature from a structureless continuous background to some well-defined bands, it should be of magnetic origin, too. There is some similarity to the two-magnon Raman scattering in NiF_2, which persists well above the Néel temperature.[24] However, this interpretation leads to some difficulties in explaining the appearance of the structure below 50 K, since a drastic change in the two-magnon scattering should be related to a magnetic phase transition, which does not occur in VCl_2. On the other hand, the anomalous scattering of VBr_2 decreases gradually with increasing temperature and does not seem to be related to the temperature dependence of the sharp absorption lines in the visible absorption spectrum.

Taking into account all the experimental observations we would like to propose the following physical picture for the anomalous Raman scattering of VBr_2 and VCl_2. A local magnetic order persisting even in a thermally disordered spin phase leads to the existence

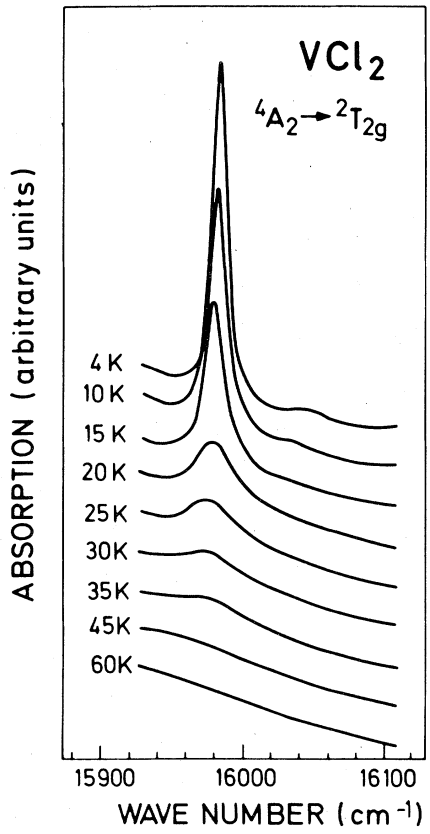

FIG. 17. Disappearance of a sharp line in the visible absorption spectrum of VCl_2 with increasing temperature.

of low-energy paramagnons and localized high-energy antiferromagnons. The sharp (magnon-assisted) lines appearing in the crystal-field spectra below a relatively well-defined temperature at which no anomalous features are observed in the magnetic susceptibility, are indicative of a local order formation. The long-range disorder now yields a Raman activity for all phonons of any wave vector $\vec{q}$ via the exchange modulation mechanism and via the elastic (Bragg) scattering in the spin system at wave vector $-\vec{q}$. As a consequence, a continuum spectrum similar to the total density of states, but weighted by a q-dependent coupling strength, should be superimposed onto the sharp one-phonon lines associated with ordinary electron-phonon interaction. This is what we actually observed in the low-temperature Raman spectra of VBr_2 and VCl_2. However, as can be seen from Fig. 16, the low-temperature Raman spectra and the calculated one-phonon density of states coincide reasonably well by allowing for a shift of the latter towards lower frequencies. From this shift, however, the $(q=0)$ E_g and A_{1g} phonon modes are exempted. Good agreement is found if we shift the calculated spectra by $\Delta = 16$ cm^{-1} for VCl_2 and by $\Delta = 10$ cm^{-1} for VBr_2 to lower frequencies. There is, of course, a certain ambiguity in the actual amount of the shift. To allow for a better comparison, in Fig. 16 the A_{1g} and E_g phonons are indicated by broken lines. The A_{1g} line in VCl_2 is displaced by more than 16 cm^{-1} with respect to the calculated spectrum. This is due to the fact that the calculated A_{1g} frequency is 5 cm^{-1} too small compared with the experimental value which has to be added to the temperature shift of 4 cm^{-1}. Thus, considering also this 4-cm^{-1} shift of the A_{1g} phonon towards higher frequencies upon cooling from 300 to 4 K, the total shift amounts to $16+5+4=25$ cm^{-1}.

Since in antiferromagnetic transition metal compounds the two-magnon scattering is known to dominate the one-magnon process,[24,25] we consider a phonon self-energy renormalization due to an interaction with two-magnon processes. This one-phonon two-magnon interaction is given by

$$H_{\rm int}=\sum_{qk} j_{q,k,q-k}(b_q^\dagger+b_q)(\alpha_{\uparrow k}^\dagger+\alpha_{\uparrow k})(\alpha_{\downarrow q-k}^\dagger+\alpha_{\downarrow q-k}) \ , \tag{5}$$

where $\alpha_{\uparrow k}^\dagger$, $\alpha_{\downarrow k}^\dagger$, $\alpha_{\uparrow k}$, $\alpha_{\downarrow k}$, $b_q^\dagger$, and b_q are magnon (α) and phonon (b) creation and annihilation operators and $j_{q,k,q-k}$ the corresponding coupling constants. The magnon operators $\alpha_{\uparrow k}^\dagger+\alpha_{\uparrow k}$ can be written as a linear combination of the spin operators $\vec{S}_m$,[25,26] and therefore $H_{\rm int}$ takes the form

$$H_{\rm int}=(2SN)^{-1}\sum_{mm',\alpha\beta} S_m^\alpha S_{m'}^\alpha \sum_q (b_q^\dagger+b_q) \times \sum_k j_{q,k,q-k} C_{mm'\alpha\beta}(k,q-k) \ , \tag{6}$$

where the coefficients $C_{mm'\alpha\beta}(k,q-k)$ depend on the particular spin structure.

By identifying the sum over k with the derivative of the (nonisotropic) exchange constant $J_{mm',\alpha\beta}$ with respect to the phonon normal coordinated A_q, we obtain

$$\left(\frac{8\hbar S^2}{\mu\omega}\right)^{1/2}\frac{\partial J_{mm',\alpha\beta}}{\partial A_q}\equiv\sum_k j_{q,k,q-k}C_{mm'\alpha\beta}(k,q-k) \ , \tag{7}$$

where μ is a reduced mass for the phonon under consideration.

The lowest-order contribution to the one-phonon self-energy, represented by a two-vertex diagram [Fig. 8(g)], is given by

$$\Sigma(\omega_q)=\frac{36}{\hbar^2}\sum_k |j_{q,k,q-k}|^2 \bar{G}^{(2)}_{k,q-k}(\omega) \ , \tag{8}$$

where $\bar{G}^{(2)}_{k,q-k}$ is the two-magnon Green's function,

identical to the two-phonon Green's function given by Eq. (1) with the magnon frequencies $\bar{\omega}_k$ replacing the phonon frequencies ω_k. The spectral shift $\Delta(\omega_q) = \mathrm{Re}\sum(\omega_q)$ of the observed phonon frequencies obviously depends on the position of ω_q with respect to the poles of the magnetic excitation spectrum. The low-energy paramagnons contribute a positive $\Delta(\omega_q)$. Because of the factor

$$(\omega_k + \omega_{q-k}) \times (n_k + n_{q-k} + 1) \ ,$$

this would be relatively small but strongly temperature dependent. The actual observation of a negative and weakly temperature dependent $\Delta(\omega_q)$ is indicative of the occurrence of two optical magnon states with total energy $\hbar(\bar{\omega}_k + \bar{\omega}_{q-k})$ in the region around the maximum phonon frequency, in agreement with the local order hypothesis. We note that in the absence of long-range order $\partial J_{mm'\alpha\beta}/\partial A_q$ is practically zero for small q values, because of disorder-induced cancellations. Finite contributions occur for q larger than π divided by the coherence length of the local magnetic order. In this case, taking

$$j_{q,k,q-k}/2\hbar\pi c \sim 10 \ \mathrm{cm}^{-1} \ ,$$

$$\bar{\omega}_k \sim \bar{\omega}_{q-k} \sim 150 \ \mathrm{cm}^{-1} \ ,$$

$$\omega_q^2 << (\bar{\omega}_k + \bar{\omega}_{q-k})^2 \ ,$$

and

$$n_k \sim n_{q-k} \sim 0$$

we estimate $\Delta(\omega_q) \sim 6 \ \mathrm{cm}^{-1}$. This has the appropriate order of magnitude and could therefore explain why the continuum spectrum (mainly due to short wavelength phonons and assisted by a Bragg scattering in the spin system) is shifted to lower frequencies with respect to $(q = 0)$ E_g and A_{1g} modes which are activated by the purely orbital electron-phonon mechanism. The tendency to a smaller shift for the heavier halogen atoms (Fig. 16) indicates that the renormalization of the zone-boundary phonons in VI_2 should be of the order of only a few wave numbers. This shift, however, is within the accuracy of the calculated phonon frequencies and thus has been neglected in the discussion in Sec. IV A.

Another low-temperature feature is found in VBr_2 in connection with the A_{1g} phonon. While the original A_{1g} line ($\sim 160 \ \mathrm{cm}^{-1}$) decreases in intensity upon cooling, another sharp line with a small sideband emerges at a slightly higher frequency (see Fig. 16). This might be interpreted in the following way: The increasing local order produces an increasing number of metal atoms seeing an identical spin arrangement in their neighborhood. Via the spin-phonon interaction this can lead to a small renormalization of the phonon frequency compared to those atoms having a completely random spin environment.

V. SUMMARY

The low-temperature Raman spectra of VCl_2, VBr_2, and VI_2 show features in addition to the two group-theoretically allowed modes. In all three cases we have attributed the additional scattering to a spin-dependent electron-phonon coupling which is given by a modulation of the exchange interaction. The difference in the Raman spectra of VI_2 compared with VBr_2 and VCl_2 are due to their different magnetic properties. VI_2 undergoes an antiferromagnetic phase transition at 15 K causing a folding of the phonon branches because of the smaller magnetic Brillouin zone. Only some selected new Γ modes, giving a nonzero modulation of the exchange interaction, can be observed by Raman scattering. VBr_2 and VCl_2 exhibit no long-range magnetic order down to 4.2 K. In this case, the spin-phonon coupling is effective within a local magnetic order, whereas the long-range disorder lifts the momentum conservation. Therefore, the additional anomalous Raman scattering resembles a one-phonon density of states. The shift of the observed spectra to lower frequencies with respect to the calculated, unrenormalized one-phonon density of states can be explained by a self-energy renormalization due to the spin-phonon coupling mechanism.

Due to the small dispersion of the phonon branches, we observe sharp two-phonon spectra in VCl_2, VBr_2, and VI_2. Therefore, these spectra can readily be assigned by the corresponding combination bands. We find an appreciable shift of the measured spectra with respect to the calculated two-phonon combinations. Some qualitative arguments for this shift are given.

ACKNOWLEDGMENTS

The authors are grateful to A. Simon, who initiated this work, to G. Lamprecht and E. Schönherr for the sample preparation, to J. C. Picoche and G. Abstreiter for cooperation in the magnetic-field-dependent measurements, and to L. Reatto, H. Bilz, and M. Cardona for many useful discussions.

*Present address: II. Physikalisches Institut, Universität Köln, Federal Republic of Germany.
†Permanent address: Technical University of Athens, Athens, Greece.
‡Permanent address: Gruppo Nazionale di Struttura della Materia del CNR, Istituto di Fisical dell' Universita, Milano, Italy.

[1]D. J. Lockwood, J. Opt. Soc. Am. 63, 374 (1973).
[2]J. C. Christie, I. W. Johnstone, G. D. Jones, and K. Zdansky, Phys. Rev. B 12, 4656 (1975).
[3]I. W. Johnstone, D. J. Lockwood, and G. Mischler, J. Phys. C 11, 2147 (1978).
[4]I. W. Johnstone, D. J. Lockwood, G. Mischler, J. R. Fletcher, and C. A. Bates, J. Phys. C 11, 4425 (1978).
[5]D. J. Lockwood, I. W. Johnstone, G. Mischler, and P. Carrara, Solid State Commun. 25, 565 (1978).
[6]G. Mischler, M. C. Schmidt, D. J. Lockwood, and A. Zwick, Solid State Commun. 27, 1141 (1978).
[7]D. J. Lockwood, D. Bertrand, P. Carrara, G. Mischler, D. Billerey, and C. Terrier, J. Phys. C 12, 3615 (1979).
[8]G. Güntherodt, R. Merlin, and P. Grünberg, Phys. Rev. B 20, 2834 (1979), and references therein.
[9]S. R. Kuindersma, C. Haas, J. P. Sanchez, and R. Al, Solid State Commun. 30, 403 (1979).
[10]K. R. A. Ziebeck and J. C. G. Houmann, in *Proceedings of the Conference on Neutron Scattering, Pt. II, Gatlinburg* (U.S. Dept. Commerce, Springfield, Va., 1976), p. 840.
[11]A. Frey and G. Benedek, Solid State Commun. 32, 305 (1979).
[12]G. Benedek and A. Frey, Phys. Rev. B 21, 2482 (1980).
[13]G. Güntherodt, W. Bauhofer, and G. Benedek, Phys. Rev. Lett. 43, 1427 (1979).
[14]C. Cros, M. Niel, G. Le Flem, M. Pouchard, and P. Hagenmüller, Mater. Res. Bull. 10, 461 (1979).
[15]M. Niel, C. Cros, G. Le Flem, M. Pouchard, and P. Hagenmüller, Nouveau J. Chim. 1, 127 (1977).
[16]G. Lamprecht and E. Schönherr, J. Cryst. Growth 49, 415 (1980).
[17]W. E. Smith, J. Chem. Soc. Dalton Trans. 1972, pt. 2, p. 1634.
[18]H. Bilz, in *Correlation Functions and Quasiparticle Interactions in Condensed Matter,* edited by I. Woods Halley (Plenum, New York, 1978), p. 483.
[19]H. Borik, Phys. Status Solidi 31, 145 (1970).
[20]A. S. Barker, Jr., and A. J. Sievers, Rev. Mod. Phys. 47, Suppl. 2, S1 (1975).
[21]P. J. Brown, K. R. A. Ziebeck, and C. Escribe, J. Magn. Magn. Mater. 15–18, 515 (1980).
[22]W. van Erk and C. Haas, Phys. Status Solidi (b) 71, 523 (1975).
[23]G. Benedek and W. Bauhofer (unpublished).
[24]P. A. Fleury, Phys. Rev. 180, 591 (1969).
[25]P. A. Fleury and R. Loudon, Phys. Rev. 166, 514 (1968).
[26]E. Rastelli, A. Taggi, and L. Reab, Physica B 97, 1 (1979).